Available online at www.sciencedirect.com
ScienceDirect
Journal of Catalysis 251 (2007) 182–188
JOURNAL OF CATALYSIS
www.elsevier.com/locate/jcat

Novel, efficient hollow zeolitically microcapsulized noble metal catalysts

Nan Ren, You-Hao Yang, Jiang Shen, Ya-Hong Zhang, Hua-Long Xu, Zi Gao, Yi Tang *

Department of Chemistry, Shanghai Key Laboratory of Molecular Catalysis and Innovative Materials and Laboratory of Advanced Materials, Fudan University, Shanghai 200433, People's Republic of China

Received 14 February 2007; revised 21 June 2007; accepted 7 July 2007

Available online 24 August 2007

Abstract

Hollow zeolitically microcapsulized (HZMC) catalysts with encapsulated noble metal nanoparticles, such as Pt and Ag, have been successfully fabricated through a hydrothermal transformation process. A series of catalytic oxidation reactions of alcohols were performed both on HZMC catalysts and on commercial catalysts, such as Pt/SiO_2 and Pt/Al_2O_3. The HZMC catalysts exhibit good reactant selectivity due to the existence of a zeolitic shell. More interestingly, the HZMC catalysts retained most of their reactivity even in the presence of a significant amount of poison contaminants (>5 vol%), whereas the reactivity on commercial catalysts was quickly quenched under the same conditions. Furthermore, the HZMC catalysts could be recycled for at least 6 runs without losing their activity, whereas the commercial catalysts deactivated rapidly with the recycling. The unique reactant-selectivity, poison-resistance, and reusability of the HZMC catalysts demonstrate that the strategy of zeolitic encapsulation for noble metal catalysts is effective and applicable in practice.

Keywords: Hollow microcapsulized catalyst; Noble metal nanoparticles; Encapsulation; Zeolite; Catalysis

1. Introduction

Currently, the encapsulation of catalytic active species into a selectively penetrable shell to form hollow microcapsulized catalyst has become a new strategy in the domain of catalyst design [1–3]. It is believed that the use of such a molecular-recognizable shell could not only improve the selectivity of the catalyst, but also protect the encapsulated active species. Recently, Ikeda et al. [4] developed a new type of carbon-encapsulated platinum catalyst displaying outstanding reusability in a series of liquid-phase hydrogenation reactions compared with the conventional active carbon-supported platinum catalysts. Shchukin et al. [5] encapsulated the bovine serum albumin in a shell of Fe_3O_4-modified polyelectrolyte microcapsules, realizing the so-called "active protein defense" systems toward hydroperoxide in the outer environment. Very recently, we invented a novel method to prepare hollow zeolitic microcapsules through hydrothermal transformation of nanozeolite-seeded mesoporous silica spheres (MSS) [6–9], and an interesting Pd@zeolite microcapsular reactor has been fabricated to achieve an encaged quasi-homogeneous Heck coupling reaction [10]. The Pd@zeolite catalyst exhibits good reusability due to the unique antileaching ability of its zeolitic shell toward the active intermediate of [Pd(II)(ArI)(solvent)(base)] or solvated Pd clusters. Moreover, the zeolitic shell also endows the catalyst with good selectivity and poison resistance due to its uniform microporosity, adjustable framework structure, and high thermal/hydrothermal stability. The molecular sieving effect of zeolites also has been used to improve the product distribution of catalysts, such as Co/SiO_2, Pt/TiO_2, and SiO_2–Al_2O_3, by coating them with a zeolitic film [11–15].

Noble metal nanoparticles have a high reactivity in many important industrial reactions, including hydrogenation, dehydrogenation, and oxidation [16–21]. However, the direct application of noble metal nanoparticles in reactions is often difficult due to their ultra-small size and high tendency toward agglomeration or sintering. The most common stabilization method, supporting noble metal nanoparticles onto carriers, often suffers from a decay of reactivity due to either the presence of a trace amount of poison in the reaction system or leaching of the active species [22,23]. Encapsulating noble metal nanoparticles in a protective shell might be an effective strategy for solving

* Corresponding author. Fax: +86 21 65641740.
E-mail address: yitang@fudan.edu.cn (Y. Tang).

0021-9517/$ – see front matter
doi:10.1016/j.jcat.2007.07.009

these problems. Due to their molecule-sieving effect and stability, zeolites could be promising candidates for such protecting shells.

In this work, we have developed hollow zeolitically microcapsulized (HZMC) catalysts with encapsulated Pt and Ag nanoparticles (denoted as Pt@S1 and Ag@S1, respectively) and an intact thin shell of silicalite-1 (denoted as S1). Industrially important oxidation reactions of alcohols were selected to illustrate the features and performance of these new catalysts. The selected reactions were of interest from both academic and practical standpoints for their green character and the challenge of selectively producing the desired products [24–29]. Experiments were designed to validate the contribution of the zeolitic shell to the reactant selectivity, poison resistance, and stability of the noble metal catalysts in both liquid and gas phases. It was found that the HZMC catalysts has sufficient mechanical strength for pelletization before use for gaseous reaction and are easily dispersed and separated when used in liquid reaction, due to their low density and micrometer size. These behaviors further ensure the easy manipulation and high efficiency of the noble metal catalysts in catalytic processes.

2. Experimental

2.1. Materials

Polydiallyldimethylammonium chloride (PDDA, Mw = 200,000, 10 wt% in water), poly(sodium 4-styrene sulfonate) (PSS, Mw = 70,000), 3-amino-propyltriethoxysilane (APS), and benzothiazole (98%) were purchased from Aldrich. (±)-1-Phenylethanol and S(−)-1-(2-naphthyl)ethanol (>98%) were purchased from Fluka. $H_2PtCl_6{\cdot}6H_2O$ was supplied by Shanghai July Chemical Company. KBH_4 (94 wt%), $AgNO_3$, tetrapropylammonium hydroxide (TPAOH, 25 wt% in water), tetraethoxy-orthosilane (TEOS), ethanol (EtOH), 3,5,5-trimethyl hexanol, and cyclohexane (C_6H_{12}) were obtained from Shanghai Chemical Reagent Company. All chemicals were used without further purification. The commercial noble metal catalyst Pt/SiO_2 (1.0 wt%, in granules, Engelhard code C3766) and Pt/Al_2O_3 (5.0 wt%) were obtained from Aldrich and Johnson Matthey, respectively. Both of the commercial catalysts were crushed before use.

2.2. Catalyst preparation

The MSS template was synthesized according to the procedure reported by Grun et al. [30], and its pore channels were modified with NH_2 groups through the method reported in our previous work [31]. The NH_2-modified step was necessary for the introduction of a large quantity of metal component into the catalysts via chelation. The noble metal species were loaded through an impregnation process. Briefly, 1 g of NH_2-modified MSS was added into 10 ml of 0.4 M aqueous solution of H_2PtCl_6 or $AgNO_3$ and stirred at room temperature for 30 min. Then the sample was reduced and calcinated according to our previous work [10]. The HZMC catalysts with encapsulated Pt and Ag nanoparticles were prepared by a two-step hydrothermal treatment in a Teflon-lined stainless steel autoclave [10] after the nanoparticle loaded-MSS was seeded with silicalite-1 nanocrystals [32] via a layer-by-layer procedure [6–9]. All of the organic ingredients in the samples were removed by calcination in air at 550 °C for 6 h before the catalytic tests. For comparison, the zeolitic microcapsules without encapsulated species were fabricated according to our previous method [9].

2.3. Catalyst characterization

The scanning electron microscopy (SEM) and transmission electron microscopy (TEM) images of the catalysts were obtained on Philips XL30 and JEOL JEM-2010 instruments with accelerate voltages of 20 and 200 kV, respectively. The X-ray diffraction (XRD) patterns were obtained on a Rigaku D/MAX-IIA diffractometer with Cu $K\alpha$ radiation. The elemental analyses were performed by inductively coupled plasma–atomic emission spectroscopy (ICP-AES). The surface areas of the samples were determined from the nitrogen sorption isotherms at −196 °C using a Micromeritics ASAP 2010 system. X-ray photoelectron spectroscopy (XPS) was carried out with a Perkin–Elmer PHI 5000C ESCA system using Al $K\alpha$ radiation (1486.6 eV) at a power of 250 W. The pass energy was set at 93.9 eV, and the binding energies were calibrated by using contaminant carbon at a BE of 284.6 eV. All samples were heavily ground to expose the Pd species before XPS measurement. Thermogravimetric analysis (TGA) was performed on a Perkin–Elmer TGAT thermal analysis system in air (50 ml min^{-1}) with a heating rate of 10 K min^{-1}. Ultraviolet–visible (UV–vis) spectra were measured with a Shimadzu UV-2450 UV–vis spectrometer.

2.4. Adsorption tests

The adsorption test of benzothiazole on various catalysts was conducted following our previously reported method [10]. The completeness of the zeolitic shell in HZMC catalyst could be detected by comparing the adsorption amount of benzothiazole on HZMC catalyst (Pt@S1 or Ag@S1) and the corresponding shell-crashed samples (denoted as C-Pt@S1 and C-Ag@S1, respectively). The adopting amount of the catalysts was kept at 30 mg, and 30 ml of an ethanolic solution of benzothiazole with a concentration of 3.0×10^{-5} M was used as the adsorbate.

2.5. Catalytic oxidation

The oxidation of aromatic alcohol in liquid phase was conducted as follows: Pt@S1, C-Pt@S1, or commercial catalysts with the same Pt amount of 0.0194 mmol (corresponding to 40 mg of Pt@S1 or C-Pt@S1, 375 mg of Pt/SiO_2, or 75 mg of Pt/Al_2O_3) was added into a mixture containing 1 g of aromatic alcohol [(±)-1-phenylethanol, **1**, or S(−)-1-(2-naphthyl)ethanol, **2**] and 30 ml of cyclohexane. The reaction was carried out at 80 °C with an air flow of 40 ml/min under stirring. The products were analyzed by high-performance liquid chromatography.

The oxidation of aliphatic alcohol in the gas phase was conducted as follows. First, 30 mg of the catalyst (Ag@S1, C-Ag@S1 or blank zeolitic microcapsules without silver) was packed into a continuous-flow fixed-bed reactor. The reaction was run under atmospheric pressure with oxygen as the oxidant and nitrogen as the diluent gas. The volume ratio of oxygen to nitrogen was 1:15. The molar ratio of O_2 to alcohol (ethanol, **3**, or 3,5,5-trimethyl hexanol, **4**) was 0.6. The liquid hourly space velocity was kept at 66.7 $g_{alcohol}\, g_{catalyst}^{-1}\, h^{-1}$, and the reaction temperature varied from 220 to 380 °C. The products were analyzed by an online gas chromatograph.

The poison-resistance test was conducted by adding 4 ml of poison (benzothiazole) into the reaction solution for liquid-phase reaction **I** after the reaction was run for 1 h, or injecting benzothiazole into the reactant with a volume concentration of 5% for gas-phase reaction **III** after the reaction was run at 300 °C for 2 min.

3. Results and discussion

3.1. Characterization of HZMC catalyst

Fig. 1 depicts SEM images of Pt@S1 and Ag@S1 obtained by a two-step hydrothermal synthesis followed by calcination at 550 °C. Both of the catalysts presented with a uniform spherical morphology with the coarse outer surface composed of closely packed zeolite nanocrystals. The insets of Fig. 1 show their hollow structures of about 1 μm in diameter and zeolitic shells about 200 nm thick. The TEM images at higher magnification (Fig. 1, insets) clearly show the highly dispersed nanoparticles of Pt (22 nm) or Ag (11 nm) inside the hollow cores. Table 1 lists the textural properties and metal contents of the synthesized HZMC catalysts. It can be seen that both samples have specific surface areas as high as that of typical silicalite-1 [33], indicating the clear pore opening of micropores in the zeolitic shell after calcination.

The intactness of the zeolitic shell and complete encapsulation of noble metal nanoparticles within HZMCs were proved by adsorption of benzothiazole molecules. Because the adsorption of benzothiazole on noble metals via chelation is irreversible and its molecular size is larger than that of the micropores in the zeolitic shell, benzothiazole is an effective probe for detecting the location of the noble metal species in the HZMC catalysts [10]. The adsorption of benzothiazole on whole (Ag@S1 and Pt@S1) and crushed HZMC catalysts (C-Ag@S1 and C-Pt@S1) was measured under the same conditions. As expected, the amounts of benzothiazole adsorbed on C-Pt@S1 and C-Ag@S1 with exposed noble metal nanoparticles reached about 6 and 2 mg/g, respectively, in 20 min, whereas the amount adsorbed on the whole HZMC samples remained negligible even after 1 h. Furthermore, an XPS experiment was carried out on the filtered catalyst after the adsorption of benzothiazole (Fig. 2). In contrast to the fresh catalyst, in which Pt was typically zero valence [centered at 71.8 eV for Pt $4f_{7/2}$ (Fig. 2a)], the C-Pt@S1 sample exhibited a shift of Pt $4f_{7/2}$ peak to 71.0 eV after the adsorption of benzothiazole (Fig. 2b), indicating the surface coverage of the heterocyclic

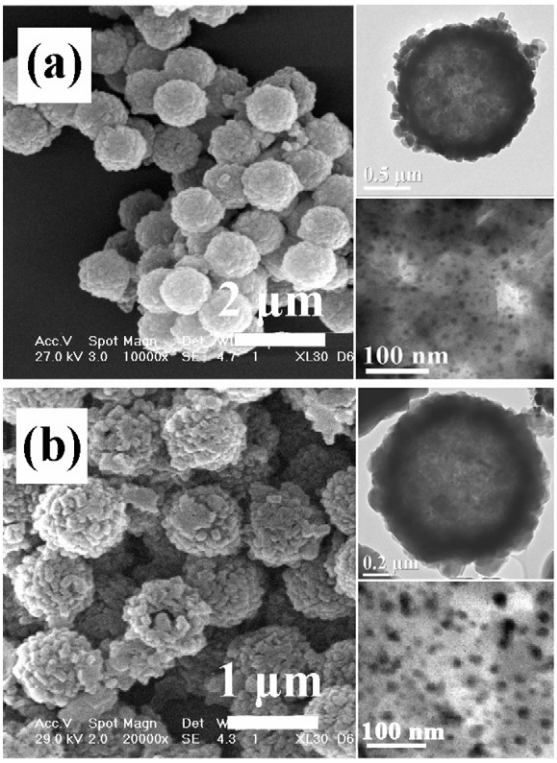

Fig. 1. SEM images of HZMC catalysts of Ag@S1 (a) and Pt@S1 (b). The insets in (a) and (b) are their corresponding TEM images at different magnifications.

Table 1
Textural properties of HZMC catalysts and commercial catalysts

Catalyst	Surface area (m^2/g)[a]	Metal content (wt%)[b]
Pt@S1	364	9.5
Ag@S1	352	2.0
Pt/SiO_2	257	1.0
Pt/Al_2O_3	104	5.0

[a] Calculated by BET method.
[b] Determined by ICP-AES method.

molecules onto the Pt nanoparticles via chelation. However, for the sample with intact zeolitic shell (Pt@S1), the peak of Pt $4f_{7/2}$ remained nearly unchanged after benzothiazole adsorption (Fig. 2c). These phenomena indicate that the noble metal nanoparticles in HZMC catalysts were well encapsulated within the hollow center of the zeolitic capsule, and this could be the reason for the enhanced poison resistance of the catalysts in the reaction, as we describe in the following sections.

The XRD patterns of Pt@S1 and Ag@S1 samples are shown in Fig. 3. Besides the characteristic diffraction peaks assigned to the silicalite-1 shell, those corresponding to the crystalline noble metal nanoparticles also can be easily distinguished in the patterns. Fig. 4 shows the TG analysis results of the as-synthesized HZMC catalysts of Pt@S1 and Ag@S1 before calcination. Both of the catalysts exhibited two weight loss steps at ca. room temperature, ∼200 °C, and 200–500 °C, which can be ascribed to the loss of adsorbed water and the further combustion of organic template in the zeolitic micropores (TPAOH), respectively [34]. It is very interesting that the Pt@S1 lost its

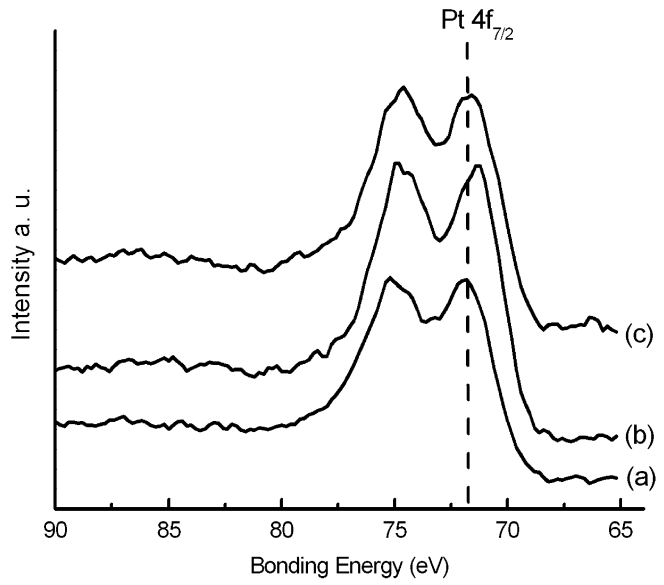

Fig. 2. XPS spectra of the Pt $4f_{7/2}$ of C-Pt@S1 before (a) and after (b) benzothiazole adsorption, and that of the shell-intact Pt@S1 (c) after adsorbing benzothiazole and then being washed with ethanol and crushed. The concentration of benzothiazole is 17 wt% in ethanol.

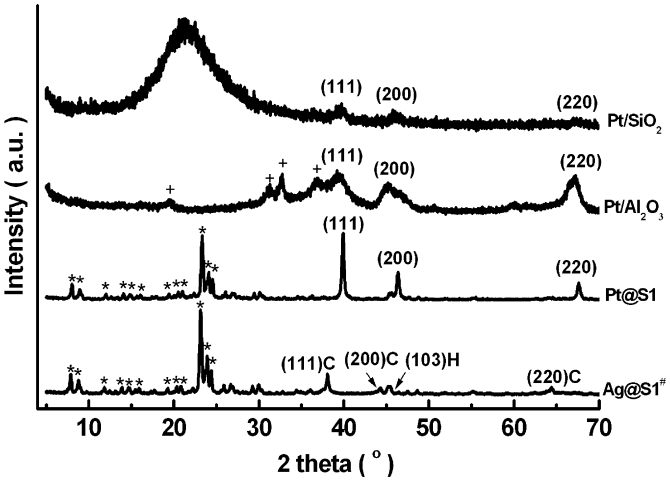

Fig. 3. XRD patterns of HZMC catalysts and commercial catalysts. The characteristic peaks attributed to zeolite are indicated by *. H and C in the XRD pattern of Ag@S1 represent the hexagonal (H) and cubic (C) phases of Ag.

TPAOH far more quickly than Ag@S1; this might be caused by the catalytic effect of Pt species on the combustion of the organic compounds. This phenomenon is in accordance with the result reported in the literature [35], where the Pt-containing mesoporous silica lost its surfactant template very quickly.

3.2. Catalytic behavior

3.2.1. Catalytic behavior in liquid phase

The shape-selectivity of the zeolitic shell on Pt@S1 catalysts was proved by the oxidation reactions of two aromatic alcohols with different molecular sizes (reaction **I** and **II**) in liquid phase. For comparison, the shell-crushed Pt@S1 (C-Pt@S1), Pt/SiO_2 (Engelhard, C3766), and Pt/Al_2O_3 (Johnson Matthey)

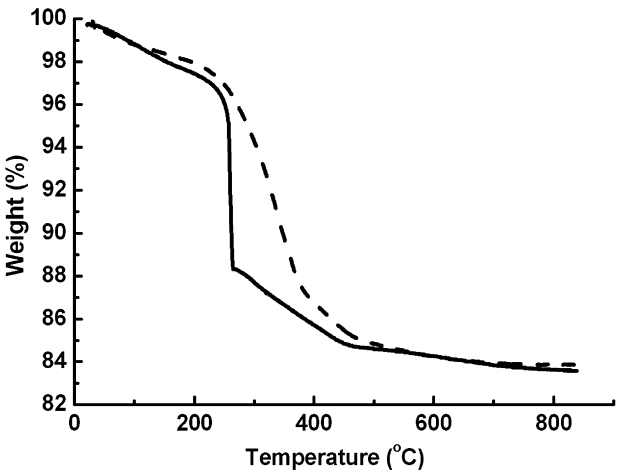

Fig. 4. TG curves of as-synthesized Pt@S1 (solid line) and Ag@S1 (dash line).

samples were also tested under the same reaction conditions. The textural properties, noble metal contents, and XRD patterns of the Pt/SiO_2 and Pt/Al_2O_3 catalysts are presented in Table 1 and Fig. 3. The conversion-versus-time curves of all samples are shown in Fig. 5. It is clear that 1-phenylethanol (reactant **1**) with a molecular size smaller than the zeolitic micropores could be favorably oxidized on all catalysts (reaction **I**). However, for the 1-(2-naphthyl)ethanol (reactant **2**) with a larger molecular size, only the catalysts with exposed Pt nanoparticles, such as C-Pt@S1, Pt/SiO_2 and Pt/Al_2O_3, were active for the oxidation reaction (reaction **II**). The inhibition of the reaction by the intact zeolitic shell on Pt@S1 demonstrates that the zeolitic encapsulation strategy was effective in creating reactant selectivity for noble metal nanocatalysts. After encapsulation, only the reactant molecules smaller than silicalite-1 micropores could enter into the hollow center of HZMC catalysts and be catalyzed by the active species inside.

It is well known that the noble metal species have poor tolerance toward the heterocyclic compounds containing sulfur or nitrogen atoms in even trace amounts [36,37]. Thus, the poison resistance of noble metal catalysts—especially the resistance toward the polyaromatic heterocyclic molecules, which are considered the most refractory S (or N) species [38,39]—is a very attractive property. The poison-resistibility of Pt@S1, C-Pt@S1, Pt/SiO_2, and Pt/Al_2O_3 were compared by adding benzothiazole into the reaction systems after the reaction proceeded for 1 h (Fig. 6a). It can be seen from Fig. 6a that benzothiazole does not affect the activity of Pt@S1 at all. The alcohol conversion on Pt@S1 keeps increasing with reaction time in the trend just like that without poison injection (Fig. 5a). In contrast, the reactions on the other three catalysts with the exposed Pt species cease immediately, and no more new products are obtained over the next 2 h.

The leaching of noble metal species from supported catalysts is another crucial problem in liquid-phase reactions. This not only leads to a loss of catalytic activity, but also may compromise the purity of the product. Thus, a high antileaching property has always been an essential requirement for such catalysts. Fig. 6b shows the reusability of all of the catalysts tested. The activity of Pt@S1 remained nearly unchanged after

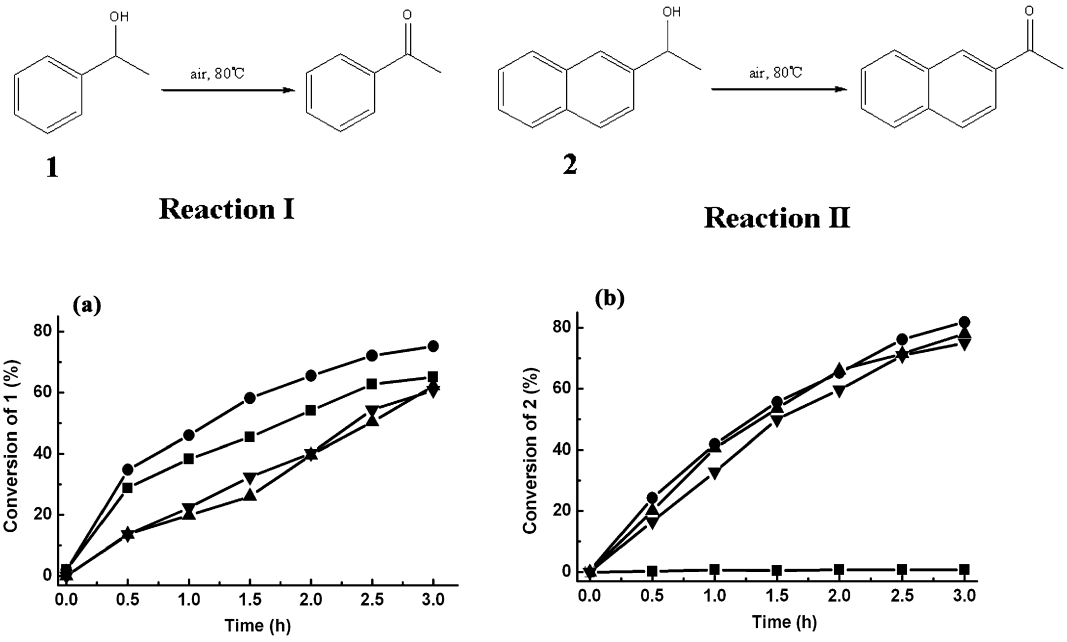

Fig. 5. The conversions of liquid-phase oxidation reactions **I** (a) and **II** (b) vs reaction time on Pt@S1 (■), C-Pt@S1 (●), Pt/SiO_2 (▲), and Pt/Al_2O_3 (▼).

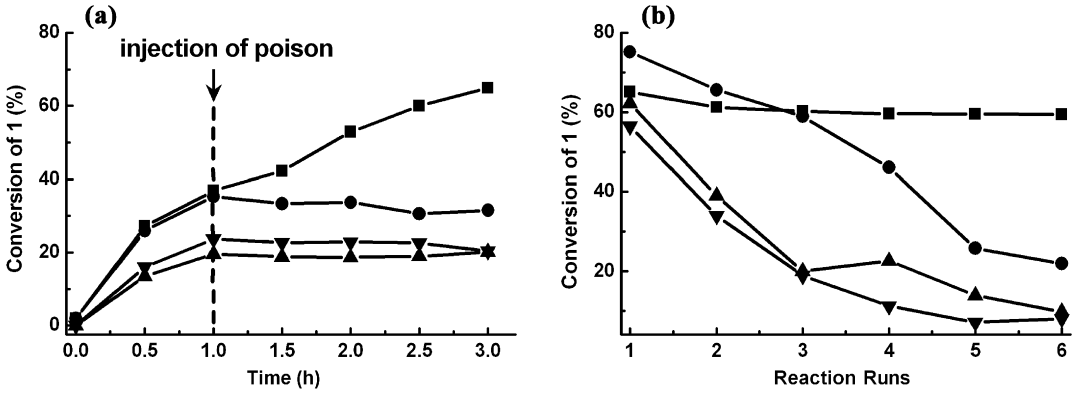

Fig. 6. The results of poison-resistance experiments (a) and the reusability tests (b) on Pt@S1 (■), C-Pt@S1 (●), Pt/SiO_2 (▲), and Pt/Al_2O_3 (▼).

use in six runs, whereas the activities of the other three catalysts decreased monotonously with reaction time. ICP-AES analysis indicates that the Pt content in Pt@S1 remained almost unchanged after reuse for 6 runs, whereas that in the other three catalyst decreased dramatically (Fig. 7). These results demonstrate that the zeolitic shell protects the encapsulated Pt nanoparticles from poisoning and also from leaching out into the solution.

In addition, our experiments demonstrate that the hollow HZMC catalysts is easier to handle in experiments than ordinary nanoparticles. They can be stably dispersed in the reaction solution due to their low density, and be easily collected after the liquid-phase reaction due to their micrometer size. These properties make them more competitive as practical catalysts.

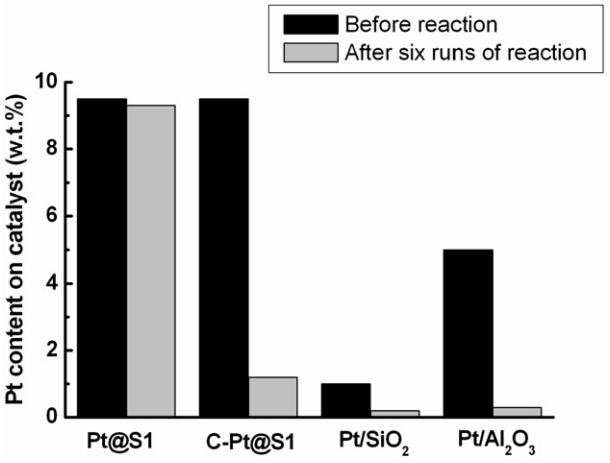

Fig. 7. The comparison of Pt content before and after six runs of reaction on various catalysts.

3.2.2. *Catalytic behavior in gas phase*

Fig. 8 illustrates the performance of an HMZC catalyst in gas-phase oxidation reactions. Here Ag@S1 was selected as the

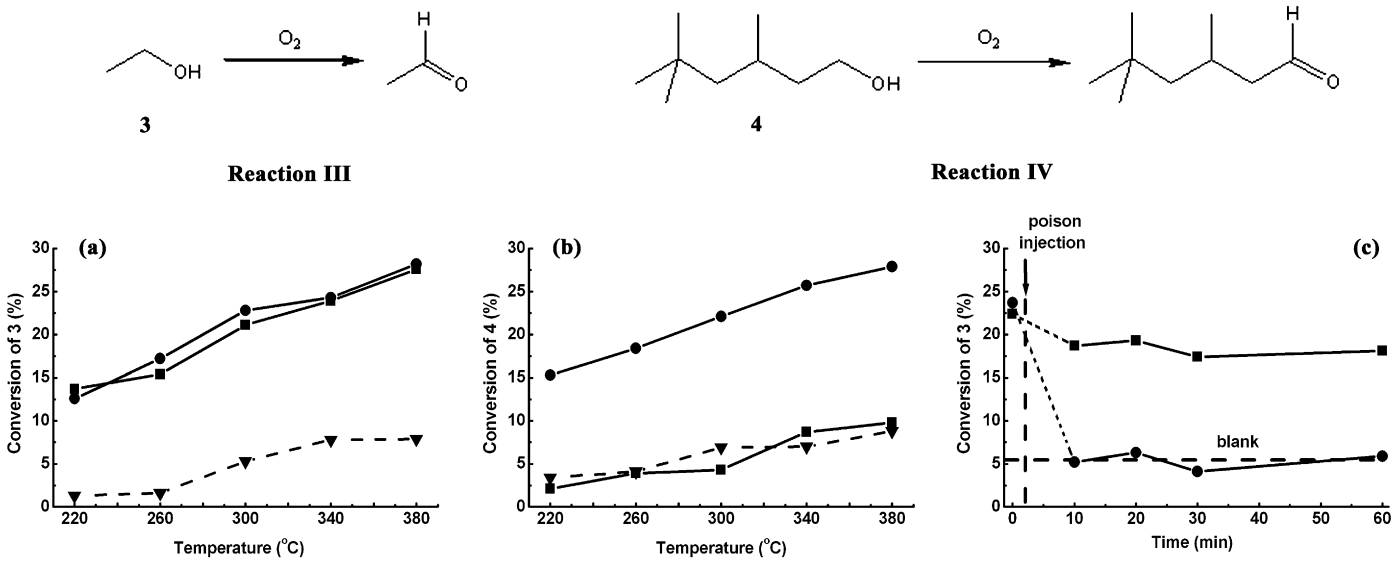

Fig. 8. The conversions of gas-phase oxidation reactions **III** (a) and **IV** (b) vs reaction temperatures for Ag@S1 (■), C-Ag@S1 (●), and the blank test (▼). (c) shows the results of poison-resistance test of Ag@S1 (■) and C-Ag@S1 (●).

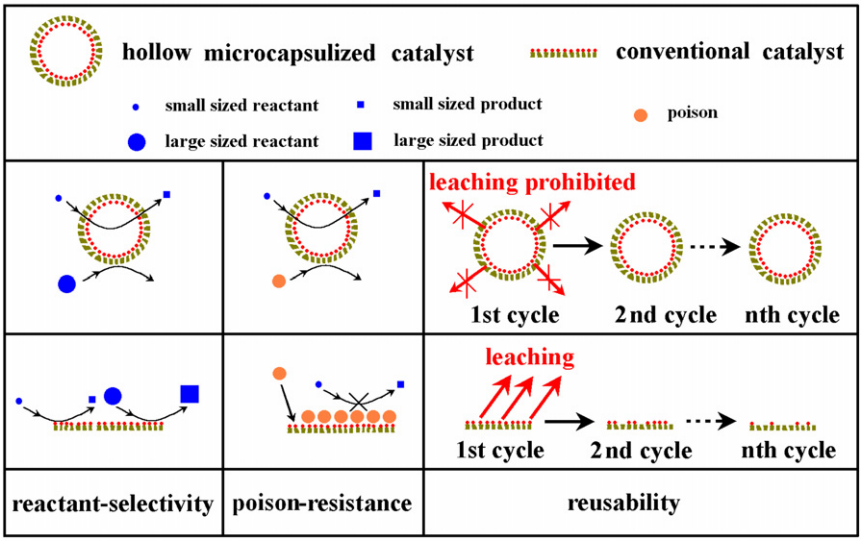

Scheme 1. Schematic illustration of the reactant-selectivity, poison-resistance ability, and reusability of HZMC catalysts.

catalyst, because silver is normally used as the alcohol oxidation catalyst in the gas phase [40,41]. The whole and crushed (C-Ag@S1) catalysts were tested under the same reaction conditions. Similar to the case in liquid-phase oxidation, both Ag@S1 and C-Ag@S1 catalysts displayed high reactivity for the small ethanol molecules (reactant **3** in reaction **III**); however, they differed significantly in terms of reactivity toward large molecules of 3,5,5-trimethyl hexanol (reactant **4** in reaction **IV**) (Figs. 8a and 8b). Ag@S1 gave a much lower oxidation activity for reactant **4**, even as low as that on blank zeolitic microcapsules without silver, whereas C-Ag@S1 exhibited high reactivity for the same reactant. More importantly, the high poison resistance of the HZMC catalyst was also reflected in the gas-phase reaction. The experiment was conducted by adding benzothiazole in the reactant after the reaction ran for 2 min. From the results in Fig. 8c, it is obvious that the addition of benzothiazole caused an immediate drop in activity of the crushed sample to the level of the blank sample, whereas that of Ag@S1 decreased by only <5% (Fig. 8c).

Note that in the gas-phase reaction experiments, the Ag@S1 catalyst was pelletized into 60–80 mesh under high pressure. The processing of the catalyst particles demonstrates that the HZMC catalysts have sufficient mechanical strength for molding and also that the molding process is harmless to the activity, selectivity and stability of the catalyst. Moreover, Figs. 8a and 5a show that both the Ag@S1 and Pt@S1 catalysts present almost the same activity for small reactants as their corresponding shell-crushed samples, especially in the gas-phase reaction. The aforementioned phenomena demonstrate that the thin zeolitic shell (∼200 nm) around the HZMC catalysts has little influence on the diffusion of small molecules. This is quite different from the behavior of the normal micrometer-sized zeo-

lites, for which good selectivity is always accompanied by high diffusion resistance and low productivity [11,42–44].

4. Conclusion

Good selectivity, poison resistance, and reusability have long been anticipated in processes involving noble metal catalysts and complex reactants. The HZMC catalysts of Pt@S1 and Ag@S1 developed in this work behave extremely well in these respects for the catalytic oxidation of alcohols in both liquid and gas phases. Their reactant selectivity, poison resistance, and reusability greatly exceed those of ordinary commercial catalysts, such as Pt/SiO_2 and Pt/Al_2O_3. The thin zeolitic shell around the HZMC catalyst is believed to be responsible for these advantages, as summarized in Scheme 1. The permeation-selective zeolitic shell prevents the large reactant and poison molecules in the reaction environment from contacting the noble metal nanoparticles encapsulated in the HZMC catalysts, leading to their good reactant selectivity and poison resistance. On the other hand, the shell prevents the encapsulated noble metal nanoparticles from leaching out of the zeolitic shell, ensuring high reusability of the catalysts. The zeolitic encapsulation strategy opens a new avenue for the design of highly efficient and economic noble metal catalysts that can meet the requirements of reaction systems of varying complexity in green and fine chemical industries.

Acknowledgments

Financial support was provided by the NSFC (20325313, 20421303, 20473022), the STCSM (05QMX1403, 05XD140-02, 06DJ14006), the Ministry of Education (104076), and the Major State Basic Research Development Program (2003CB-615807).

References

[1] I.L. Radtchenko, M. Giersig, G.B. Sukhorukov, Langmuir 18 (2002) 8204.
[2] C. Ramarao, S.V. Ley, S.C. Smith, I.M. Shirley, N. DeAlmeida, Chem. Commun. (2002) 1132.
[3] D.H. Turkenburg, A.A. Antipov, M.B. Thathagar, G. Rothenberg, G.B. Sukhorukov, E. Eiser, Phys. Chem. Chem. Phys. 7 (2005) 2237.
[4] S. Ikeda, S. Ishino, T. Harada, N. Okamoto, T. Sakata, H. Mori, S. Kuwabata, T. Torimoto, M. Matsumura, Angew. Chem. Int. Ed. 45 (2006) 7063.
[5] D.G. Shchukin, T. Shutava, E. Shchukina, G.B. Sukhorukov, Y.M. Lvov, Chem. Mater. 16 (2004) 3446.
[6] A.G. Dong, N. Ren, W.L. Yang, Y.J. Wang, Y.H. Zhang, D.J. Wang, H.H. Hu, Z. Gao, Y. Tang, Adv. Funct. Mater. 13 (2003) 943.
[7] A.G. Dong, Y.J. Wang, Y. Tang, N. Ren, Y. Zhang, Z. Gao, Chem. Mater. 14 (2002) 3217.
[8] A.G. Dong, Y.J. Wang, D.J. Wang, W.L. Yang, Y.H. Zhang, N. Ren, Z. Gao, Y. Tang, Micropor. Mesopor. Mater. 64 (2003) 69.
[9] A.G. Dong, Y.J. Wang, Y. Tang, D.J. Wang, N. Ren, Y.H. Zhang, Z. Gao, Chem. Lett. 32 (2003) 790.
[10] N. Ren, Y.H. Yang, Y.H. Zhang, R.Q. Wang, Y. Tang, J. Catal. 246 (2007) 215.
[11] N. Nishiyama, M. Miyamoto, Y. Egashira, K. Ueyama, Chem. Commun. (2001) 1746.
[12] N. Nishiyama, K. Ichioka, D.-H. Park, Y. Egashira, K. Ueyama, L. Gora, W.D. Zhu, F. Kapteijn, J.A. Moulijn, Ind. Eng. Chem. Res. 43 (2004) 1211.
[13] J. He, Y. Yoneyama, B.L. Xu, N. Nishiyama, N. Tsubaki, Langmuir 21 (2005) 1699.
[14] M. Miyamoto, T. Kamei, N. Nishiyama, Y. Egashira, K. Ueyama, Adv. Mater. 17 (2005) 1985.
[15] J.J. He, Z.L. Liu, Y. Yoneyama, N. Nishiyama, N. Tsubaki, Chem. Eur. J. 12 (2006) 8296.
[16] H. Song, R.M. Rioux, J.D. Hoefelmeyer, R. Komor, K. Niesz, M. Grass, P.D. Yang, G.A. Sormorjai, J. Am. Chem. Soc. 128 (2006) 3027.
[17] A. Corma, M.E. Domine, Chem. Commun. (2005) 4042.
[18] N. Ren, A.G. Dong, W.B. Cai, Y.H. Zhang, W.L. Yang, S.J. Huo, Y. Chen, S.H. Xie, Z. Gao, Y. Tang, J. Mater. Chem. 14 (2004) 3548.
[19] M.V. Vasylyev, G. Maayan, Y. Hovav, A. Haimov, R. Neumann, Org. Lett. 8 (2006) 5445.
[20] W.P. Zhou, A. Lewera, R. Larsen, R.I. Masel, P.S. Bagus, A. Wieckowski, J. Phys. Chem. B 110 (2006) 13393.
[21] B. Zhou, S. Herman, G.A. Somorjai, in: Nanotechnology in Catalysis, Kluwer Academic, New York, 2004, p. 138.
[22] M. Besson, P. Gallezot, Catal. Today 81 (2003) 547.
[23] A. Papp, K. Miklós, P. Forgo, Á. Molnár, J. Mol. Catal. A Chem. 229 (2005) 107.
[24] R.A. Sheldon, J.K. Kochi, Metal-Catalyzed Oxidation of Organic Compounds, Academic Press, New York, 1981, p. 1.
[25] T. Mallat, A. Baiker, Chem. Rev. 104 (2004) 3037.
[26] S.N. Sidorov, I.V. Volkov, V.A. Davankov, M.P. Tsyurupa, P.M. Valetsky, L.M. Bronstein, R. Karlinsey, J.W. Zwanziger, V.G. Matveeva, E.M. Sulman, N.V. Lakina, E.A. Wilder, R.J. Spontak, J. Am. Chem. Soc. 123 (2001) 10502.
[27] C. Keresszegi, J.D. Grunwaldt, T. Mallat, A. Baiker, J. Catal. 222 (2004) 268.
[28] J.H. Vleeming, B.F.M. Kuster, G.B. Marin, F. Oudet, P. Courtine, J. Catal. 166 (1997) 148.
[29] C. Keresszegi, T. Mallat, J.D. Grunwaldt, A. Baiker, J. Catal. 225 (2004) 138.
[30] M. Grun, C. Buchel, D. Kumar, K. Schumacher, B. Bidlingmaier, K.K. Unger, Stud. Surf. Sci. Catal. 128 (2000) 155.
[31] N. Ren, B. Wang, Y.H. Yang, Y.H. Zhang, W.L. Yang, Y.H. Yue, Z. Gao, Y. Tang, Chem. Mater. 17 (2005) 2582.
[32] J. Sterte, S. Mintova, G. Zhang, B.J. Schoeman, Zeolites 18 (1997) 387.
[33] Y.J. Wang, Y. Tang, Z. Ni, W.M. Hua, W.L. Yang, X.D. Wang, W.C. Tao, Z. Gao, Chem. Lett. (2000) 510.
[34] K.H. Gilbert, R.M. Baldwin, J.D. Way, Ind. Eng. Chem. Res. 40 (2001) 4844.
[35] P. Krawiec, E. Kockrick, P. Simon, G. Auffermann, S. Kaskel, Chem. Mater. 18 (2006) 2663.
[36] T.C. Xiao, L.D. An, W.M. Zhang, S.S. Sheng, G.X. Xiong, Catal. Lett. 12 (1992) 287.
[37] X.L. Huang, S.K. Shen, Chin. J. Catal. 24 (2003) 233.
[38] A. Niquille-Rothlisberger, R. Prins, J. Catal. 242 (2006) 207.
[39] H. Farag, K. Sakanishi, J. Catal. 225 (2004) 531.
[40] J. Shen, W. Shan, Y.H. Zhang, J.M. Du, H.L. Xu, K.N. Fan, W. Shen, Y. Tang, J. Catal. 237 (2006) 94.
[41] J. Shen, W. Shan, Y.H. Zhang, J.M. Du, H.L. Xu, K.N. Fan, W. Shen, Y. Tang, Chem. Commun. (2004) 2880.
[42] W. Zhu, F. Kapteijn, J.A. Moulijn, Micropor. Mesopor. Mater. 47 (2001) 151.
[43] C.L. Cavalcante, D.M. Ruthven, Ind. Eng. Chem. Res. 34 (1995) 177.
[44] C.L. Cavalcante, D.M. Ruthven, Ind. Eng. Chem. Res. 34 (1995) 185.